Universiteit Utrecht

Department of Physics and Astronomy
Institute for Subatomic Physics

Blastwave parameterization for Pb-Pb collisions at $\sqrt{s_{NN}} = 2.76$ TeV and $\sqrt{s_{NN}} = 5.02$ TeV

Bachelor Thesis

Laura Scheffer
Study: Natuur- en Sterrenkunde

Supervisor:

Dr. P. Christakoglou
Dutch National Institute for Subatomic Physics (NIKHEF)
Institute for Subatomic Physics at Utrecht University

January 16, 2018

Abstract

In heavy-ion collisions an extremely hot and dense state of matter, known as the quark-gluon plasma (QGP), is created. This plasma immediately cools due to a rapid expansion and the quarks and gluons form hadrons that are detected by dedicated detectors. The QGP can be described by various models, one of which is known as the blast-wave model. The blast-wave model aims to parameterize the freeze-out phase, the moment particles that are produced in the collision freely stream towards the detector, of the QGP with the use of eight parameters. In this thesis data from the ALICE collaboration is used. The data describe the centrality dependence of particle production of $\pi^{\pm}$, $K^{\pm}$ and $p(\bar{p})$ as well as the transverse momentum dependence of the harmonic flow coefficients v_2 and v_3 in Pb-Pb collision at $\sqrt{s_{NN}}$ = 2.76 TeV and $\sqrt{s_{NN}}$ = 5.02 TeV. The data are fitted with the blast-wave model and from the fit the freeze-out temperature, average transverse velocity of the system and the parameter ρ_2, related to the elliptic flow of the system, are determined. When analysing these parameters it was found that the freeze-out temperature is not affected by the energy difference, whereas the average transverse velocity of the system does indicate a modest increase with energy.

Contents

1 Introduction

In the early stages of the universe, right after the Big Bang, there was an extremely hot and dense state of matter. This matter consisted mainly of quarks -elementary particles- and gluons, that are carriers of the strong force. Due to the strong interaction the quarks and gluons are strictly confined, nevertheless in this extremely hot and dense state they were only weakly bound and free to move in the so called quark-gluon plasma (QGP). With high energy heavy-ion (such as lead) collisions in the laboratory this quark-gluon plasma can be recreated and its properties can be studied in a controlled environment.

For these high energy collisions very powerful accelerators are needed such as the Relativistic Heavy Ion Collider (RHIC) at the Brookhaven National Laboratory or the Large Hadron Collider (LHC) at CERN. In this thesis, data that was obtained from lead-lead (Pb-Pb) collisions at the LHC, for centre-of-mass energies of 2.76 TeV and 5.02 TeV, are used.

There exist various models that aim to describe properties of the QGP and one of these is the blast-wave model (see Sec. 2.3). The blast-wave model attempts to parameterize the freeze-out phase (hadronization) of the QGP. This is done by applying a blast-wave model fit to the particles transverse momentum spectra and the harmonic flow coefficients v_2 and v_3. A blast-wave model fit can be done on the spectra alone, but it is also possible to do a fit on the spectra and the harmonic flow coefficients simultaneously. In this thesis the blast-wave parameterizations for Pb-Pb collisions at $\sqrt{s_{NN}} = 2.76$ TeV and $\sqrt{s_{NN}} = 5.02$ TeV are studied. For both energies a fit on the spectra and on the spectra plus v_2 is done and the parameterization is then used to determine the freeze-out temperature and average transverse velocity of the system. The results for 2.76 TeV and 5.02 TeV are compared to study the effect of the energy on the parameter values. Finally an attempt was made to fit the spectra and both flow coefficients simultaneously, but as described in Sec. 5 this can not yet be succesfully done.

2 Theory

2.1 Standard Model

From the last century up to now ideas, theories and discoveries have led to new insights on the structure of matter. All matter is thought to be made up from fundamental (or elementary) particles that are governed by four fundamental forces. These particles and three of the forces are explained by the Standard Model (see Figure 1).

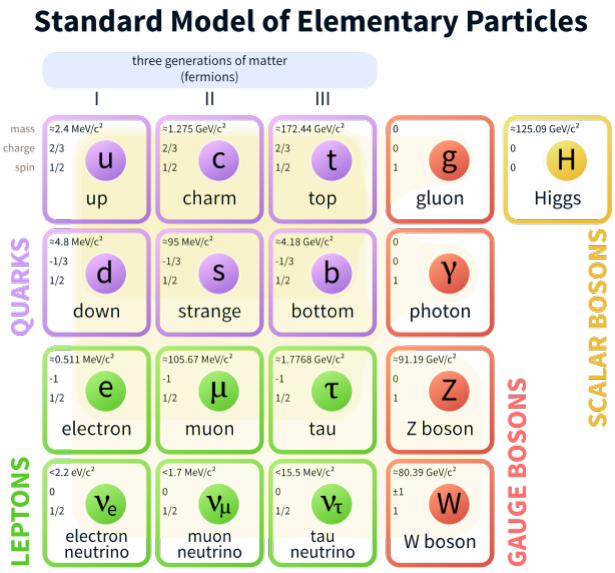

Figure 1: Representation of how the standard model orders the elementary particles into different groups. [1]

There are two types of fundamental particles quarks and leptons and each type consists of six particles that are related in pairs (so called generations). The four forces are the gravitational force, the electromagnetic force, the weak force and the strong force. The gravitational force is not included in the Standard Model, because it has proven to be difficult to fit it in. The three other forces included in the Standard Model arise from the exchange of force-carrier particles that are called bosons. Each of the forces has it's own force carrier; the electromagnetic force is carried by the photons, the weak force is carried by the W and Z bosons and the strong force is carried by the gluons.

These gluons normally confine quarks into mesons and baryons, therefore quarks can't be detected as a particle directly. However right after the Big Bang, when everything was extremely hot and dense, quarks and gluons were bound only weakly and free to move in what's called a quark-gluon plasma (QGP). Figure 2 presents a schematic view of what the phase diagram of the quantum chromodynamics (QCD, the theory of strong interactions) matter could look like.[2].

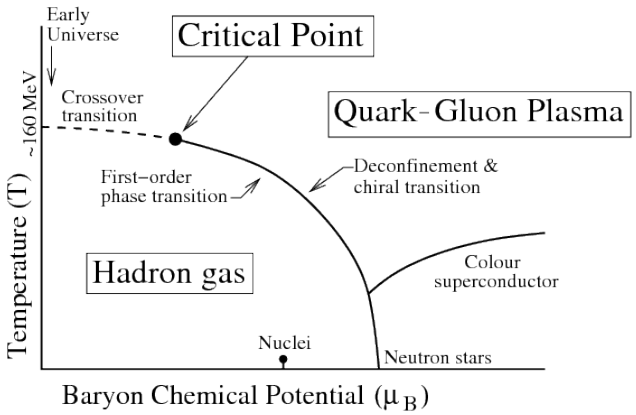

Figure 2: A QCD phase diagram. If the temperature and density are high enough there will be a transition from the hadronic phase to the quark-gluon plasma. Figure is reproduced from Ref.[3]

2.2 Heavy-ion collisions

To recreate these extreme conditions particle accelerators, such as the Large Hadron Collider (LHC) at CERN, collide heavy ions (such as lead). These collisions result in a fireball where a quark-gluon plasma is formed. This hot and dense matter expands and cools instantly and the quarks and gluons form hadrons, that scatter in every direction. The decoupling of hadrons from the bulk matter is called the freeze-out phase of the collision, this is when the hadrons start to stream freely towards the detector. These hadrons are detected and measurements are performed on them[4].

One of these measurements is the transverse momentum p_T spectra. The transverse momentum is perpendicular to the z-axis, that runs along the beam line, and therefore p_T will be zero before the collision. The p_T spectra can provide information about the bulk production (for low $p_T \lesssim 2$ GeV/c) or transport properties of the medium [5].

An other unique feature of a heavy-ion collision is centrality. Centrality is related to the initial overlap region of the two colliding nuclei. Geometrically it is defined by the impact parameter b, the distance between the centres of the two colliding nuclei, see Figure 3. A central collision corresponds to a low value of b and a peripheral collision corresponds to a large value of b. However, the impact parameter can't be measured directly, so an experimental observable needs to be related to this parameter. The multiplicity of the collision is a measurable observable that provides information about the impact parameter of the collision. High particle multiplicity relates to a central collision and low particle multiplicity relates to peripheral collisions. Centrality is expressed as a percentage of the total nuclear interaction cross-section, e.g. 10% of the most central events are the 10% that have the highest particle multiplicity[6].

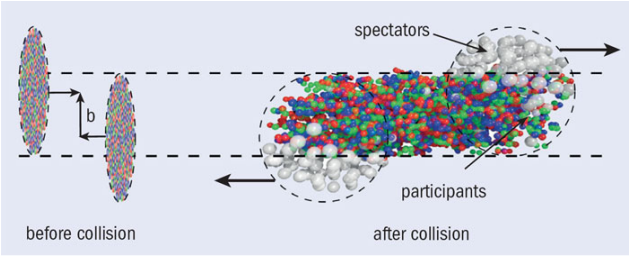

Figure 3: Left: two heavy ions before collision with impact parameter b. Right: the spectator nucleons remain unaffected while particle production takes place in the participants'zone. Figure is reproduced from Ref. [6]

2.3 Blast-Wave Model

The blast-wave model aims to parameterize the freeze-out configuration of the system based on several parameters. In this thesis the Retiere and Lisa blast-wave model (RL model, see Ref. [7]) is used, which is based on eight parameters, namely: T_{fo}, ρ_0, ρ_2, R_x, R_y, a_s, τ_0 and $\Delta\tau$. The transverse shape is controlled by the radii R_x and R_y, a_s corresponds to a surface diffuseness of the emission source, ρ_0 and ρ_2 are related to the flow rapidity of the system. The parameter τ controls the longitudal distribution.

The model assumes that the detected particles are emitted from a source element at a fixed temperature T. Moreover the source element is boosted with a transverse rapidity $\rho(x, y)$. In the case of the RL model the boost is perpendicular to the elliptical sub-shell, see Figure 4 on which the source element if found. It can be shown that the following holds for the RL model:

$$\tan(\phi_s) = \left(\frac{R_y}{R_x}\right)^2 \tan(\phi_b)$$

where ϕ_s is the spatial azimuthal angle and ϕ_b the azimuthal direction of the boost.

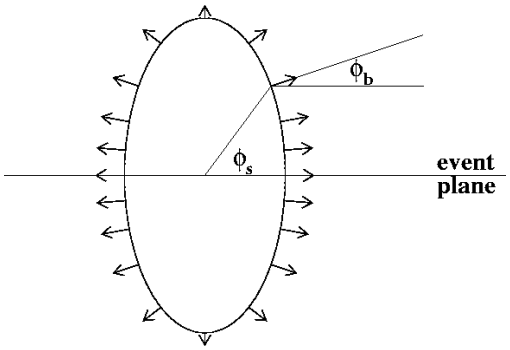

Figure 4: The source is extended out of the reaction plane if $R_y > R_x$. Arrows represent the direction and magnitude of the flow boost. In this case $\rho_2 > 0$. Figure reproduced from Ref. [7]

The boost strength depends linearly on the normalized radius $\tilde{r}$ [1] and is characterized by the parameter ρ_0. For non-central collisions the parameter ρ_2 is included in the flow rapidity. This parameter characterizes the strength of the second-order oscillation of the transverse rapidity.

$$\rho(r, \phi_s) = \tilde{r}(\rho_0 + \rho_2 cos(2\phi_b))$$

The source anisotropy is parameterized in two independent ways both affecting elliptic flow. If $\rho_2 > 0$ the boost is stronger in-plane than out-of-plane contributing to positive elliptic flow. Even if $\rho_2 = 0$ (but $\rho_0 \neq 0$) there is still contribution to positive elliptic flow when $R_y > R_x$, since this means there will be more sources emitting in-plane than out-of-plane.

The emission function of the RL model is given by

$$\begin{aligned} S(x, K) &= (S, r, \phi_s, \tau, \eta) \\ &= m_T \cosh(\eta - Y)\Omega(r, \phi_s) e^{\frac{-(\tau-\tau_0)^2}{2\Delta\tau^2}} \sum_{n=1}^{\infty} (\mp 1)^{n+1} e^{n\alpha \cos(\phi_b - \phi_p)} e^{-n\beta \cosh(\eta - Y)} \end{aligned}$$

where

$$\alpha \equiv \frac{p_T}{T} \sinh \rho(r, \phi_s)$$

$$\beta \equiv \frac{m_T}{T} \cosh \rho(r, \phi_s).$$

The transverse momentum (p_T), transverse mass (m_T), rapidity (Y), and the azimuthal angle (ϕ_p) refer to the momentum of the emitted particle. The emission function can be simplified by setting $Y = 0$. Then the p_T spectra are calculated with

$$\frac{dN}{p_T dp_T} = \int \phi_p \int d^4x S(x, K) \propto m_T \int d\phi_p \{1\}_{0,0}(K) \tag{1}$$

and v_2 is calculated through

$$v_2(p_T, m) = \frac{\int_0^{2\pi} d\phi_p \{\cos(2\phi_p\}_{0,0}(K)}{\int_0^{2\pi} d\phi_p \{1\}_{0,0}(K)}. \tag{2}$$

The RL model focuses on the shapes of the spectra and not the normalization.

[1] This is defined as $\tilde{r} = \sqrt{\frac{(rcos(\phi_s))^2}{R_x^2} + \frac{(rsin(\phi_s))^2}{R_y^2}}$

3 Large Hadron Collider

The data used for the analysis in this thesis comes from the ALICE (A Large Ion Collider Experiment) detector at the Large Hadron Collider that is part of the CERN accelerator complex. The Large Hadron Collider (LHC) is the biggest and most powerful particle accelerator in the world. The LHC consists of a 27-kilometre ring of superconducting magnets with a number of accelerating structures to boost the energy of particles along the way. Two high-energy particle beams travel in opposite directions with velocities close to the speed of light. These beams are guided by 1232 dipole magnets of 15 metres long and focused by 392 quadrupole magnets of 5-7 metres long. The beams are made to collide at four locations around the accelerator ring, corresponding to the four particle detectors: ATLAS, CMS, LHCb and ALICE[8]. The data used in this thesis was recorded by ALICE.

3.1 ALICE

ALICE is designed to study the physics of the quark-gluon plasma (QCP) and the detector is optimized to track and identify particles over a wide range of transverse momenta from 100 MeV c^{-1} to 100 GeV c^{-1}. In addition, ALICE works in an environment with large charged-particle multiplicities of approximately 2000 charged particles per rapidity unit.

ALICE consists of a central system, covering mid-rapidity ($|\eta| \leq 0.9$) over the full azimuth and several forward systems, see Figure 5. The sub-detectors in the central system are the Inner Tracking System (ITS), the Time-Projection Chamber (TPC), a Transition-Radiation Detector (TRD, for identifying electrons), the Time-Of-Flight (TOF), the Ring Imaging Cherenkov (HMPID) and an electromagnetic calorimeter PHOS. The detectors in the forward systems are the Forward Multiplicity Detector (FMD), the V0 detector, the T0 detector, the Photon Multiplicity Detector (PMD) and the Zero-Degree Calorimeters. The data in this thesis is obtained with the ITS, TPC, TOF and V0 detectors, which will be discussed in more detail below. For more detailed information about the ALICE detector see Ref. [9]. The information provided here is a short summary from this publication on the most relevant parts for this thesis, namely the detectors used to obtain the data that were used.

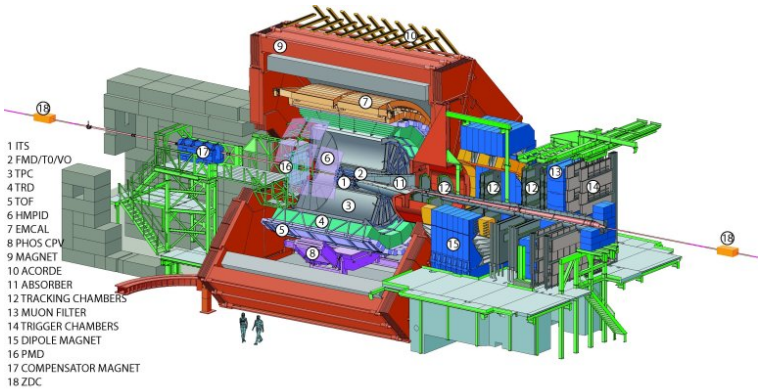

Figure 5: The layout of the ALICE detector. [10]

Inner Tracking System (ITS) The ITS is made of six cylindrical layers of silicon detectors. Due to the high particle density and to achieve the required impact-parameter resolution, Silicon Pixel Detectors (SPD) are used for the innermost two layers. The following two layers are Silicon Drift Detectors (SDD) and the two outermost layers are made with Silicon micro-Strip Detectors (SSD). The main tasks of the ITS are to localize the primary vertex with a resolution better than 100 μm and to reconstruct the secondary vertices from the decays of hyperons and the B and D mesons. It also tracks and identifies particles with low momenta with p_t down to 100 MeV/c. In addition it is used to improve the momentum and angle resolution for particles reconstructed by the TPC and to recover tracks of particles that are not reconstructed by the TPC.

Time-Projection Chamber (TPC) The Time-Projection Chamber is the main tracking detector of the central system and, together with the other detectors in the central system, provides charged-particle momentum measurements with good two-track seperation. It is also the main detector for the study of hadronic observables for both heavy-ion and pp collisions. Hadronic measurements provide information about the flavour of the particle-emitting source via the spectroscopoy of strange and multi-strange hadrons, on its space-time evolution, and extent at freeze-out via single- and two-particle spectra and correlations, and on event-by-event fluctuations. To achieve this the TPC is required to have a momentum resolution on 1% for momenta as low as 100 MeV c^{-1}, a resolution on the momentum difference of about 5 MeV c^{-1} to measure two particle correlations, have a dE/dx resolution better than 7% to identify different hadron species, and have full azimuthal coverage in order to analyse the event globally.

Time-Of-Flight (TOF) The Time-Of-Flight (TOF) is a large area array that covers the central pseudo-rapidity region ($|\eta| \leq 0.9$) in the intermediate momentum range (from 0.2 to 2.5 GeV c^{-1}). Together with the ITS and TPC it provides event-by-event identification of large samples of pions, kaons and protons. Since a large area has to be covered, there was no other choice than a gaseous detector. This gaseous detector, Multi-gap Resistive-Plate Chamber (MRPC), has a high uniform electric field. So any ionization will immediately start a gas avalanche process that will generate the observed signals on the pick-up electrodes.

V0 The V0 detector is a small angle detector that consists of two arrays of scintillator counters (V0A and V0C). The detector provides minimum-bias triggers for the central barrel detectors in pp and A-A collisions. It also serves as an indicator of the centrality of the collision via the multiplicity recorded in the event. In addition the V0 detector also participates in the measurement of luminosity in pp collisions.

4 Analysis

The analysis was performed on data from the ALICE detector for Pb-Pb collisions with centre-of-mass energies 2.76 TeV and 5.02 TeV (the former from previously published articles, [11] and [12], and the latter based on preliminary results not yet published [13]). The particles studied in this analysis are $\pi^{\pm}$, $K^{\pm}$ and $p(\bar{p})$ in different centrality ranges. These data sets were analysed with the ROOT framework, developed by CERN, and a code written in C++ that executed the blast-wave model fit. These data sets are used to plot the particles' transverse momentum spectra, with centrality ranges from 0-5% up to 80-90%, and the harmonic flow coefficients v_2 (elliptic flow) and v_3 (triangular flow) for centrality ranges from 0-5% up to 40-50%. The plots are then used as an input for the blast-wave model fit. The blast-wave fit is then done for just the spectra (referred to as "single fit" in this thesis), for both the spectra and v_2 simultaneously ("double fit") and for the spectra, v_2 and v_3 simultaneously ("triple fit"). Figure 6 presents the transverse momentum spectra for charged pions, charged kaons and (anti)protons for various centrality ranges. In like manner the plots for v_2 and v_3 Figures 7 and 8 are given, but just for few indicative centrality ranges: 0-5%, 20-30% and 40-50%. Each figure is followed by a short discussion.

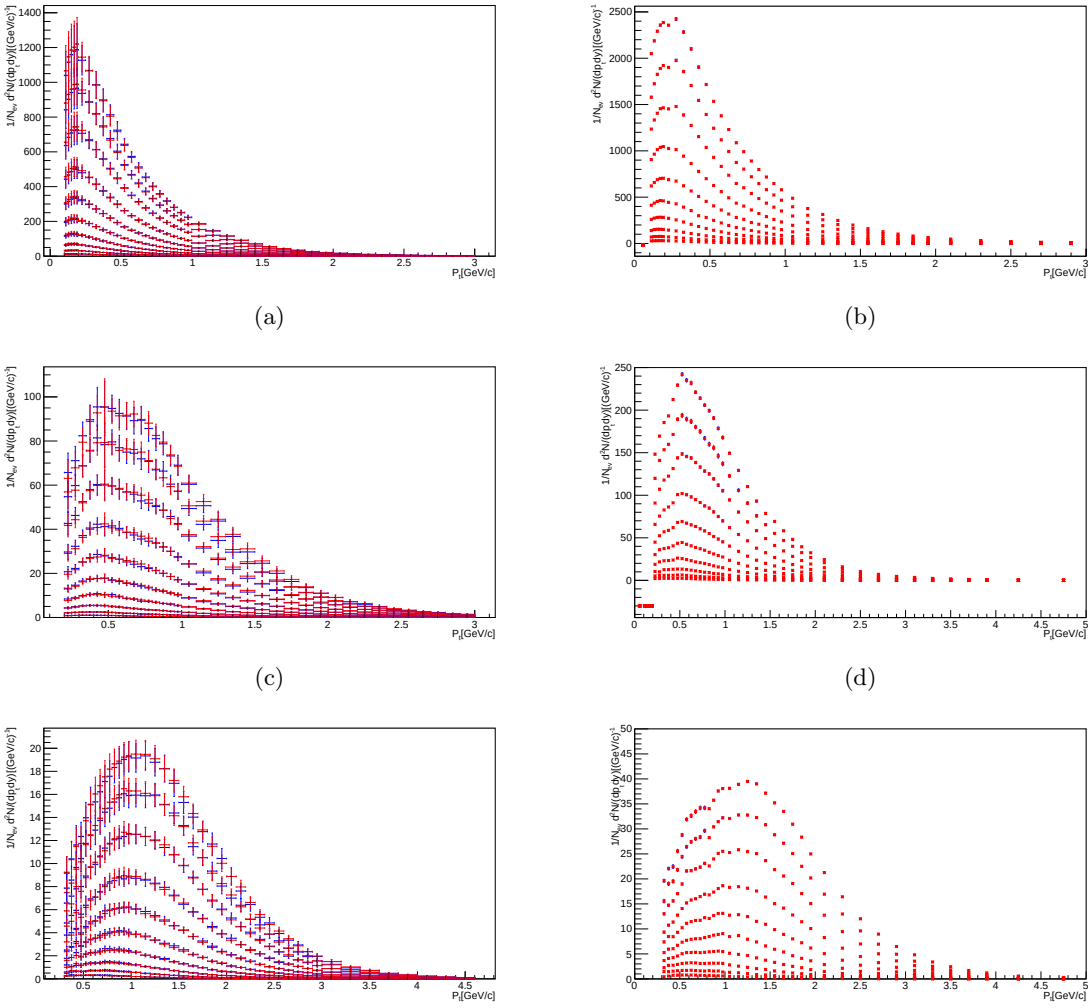

Figure 6: The particle yield for $\pi^{\pm}$, $K^{\pm}$ and $p(\bar{p})$ as a function of p_T for different centralities. The highest particle yield for each species corresponds to the most central collisions, 0-5%, and the lowest yield with the most peripheral collisions, 80-90%.

For all spectra there is a definite increase in particle yield at a higher energy, which is only to be expected due to conservation of energy. Even though the resulting fireball at $\sqrt{s_{NN}}$= 5.02 TeV is hotter and denser compared to the fireball at 2.76 TeV, it seems to be that the average transverse momentum of all charged particles is almost independent of the energy of the collision. The average p_T for these particles lies around 0.3 GeV/c. In addition the particle yield for every species falls off very rapidly as a function of p_T and it is strongly dependent on the centrality of the collision.

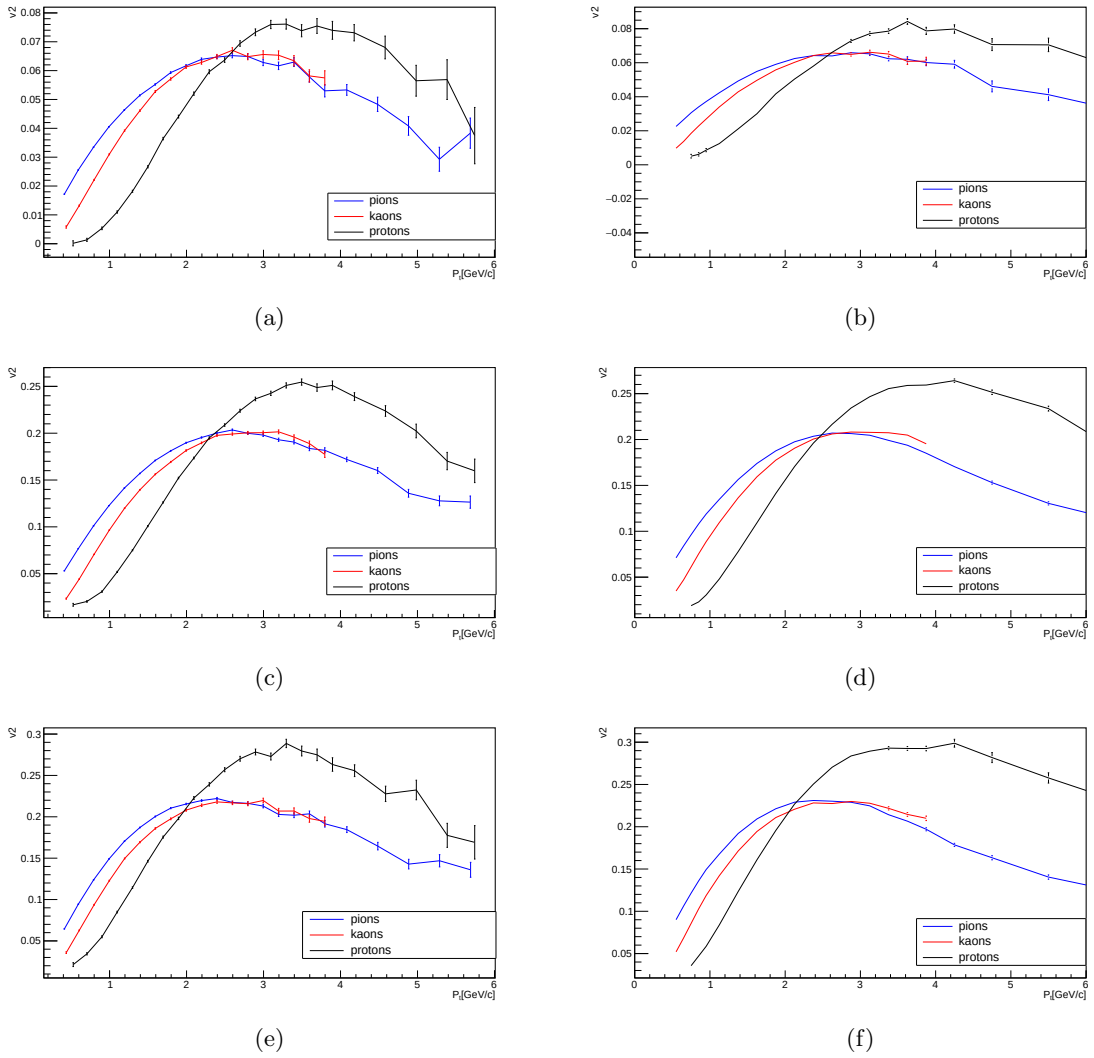

Figure 7: Elliptic flow coefficients for various centralities: (a) and (b) at 0-5%; (c) and (d) at 20-30%; (e) and (f) at 40-50%

In Figure 7 the elliptic flow coefficients as a function of transverse momentum for all particle species ($\pi^{\pm}$, $K^{\pm}$, $p(\bar{p})$) are presented. Figures 7a, 7c and 7e present the elliptic flow coefficients measured at $\sqrt{s_{NN}}$= 2.76 TeV, whereas Figures 7b, 7d and 7f are measurements at $\sqrt{s_{NN}}$= 5.02 TeV. First of all it can be noted that there is a centrality dependence of the flow coefficient, with an increasing value for v_2 for more peripheral collisions. Additionally between the semi-central (7c and 7d) and the most peripheral measurements (7e and 7f) there is no longer a significant difference in the values of v_2 for pions and kaons at both 2.76TeV and 5.02TeV. The coefficient seems to not develop any further when the collision becomes more peripheral.

Comparing the results for 2.76 TeV with those of 5.02 TeV there is no difference in the maximum values of the coefficients, which seem to indicate that this value does not depend on the energy. However there is a slight shift to higher values of p_T for the maximum value at 5.02 TeV with respect to 2.76 TeV which can be explained by the difference in the pressure gradients in the fireball. In the case of higher energies the fireball will be hotter and denser, thus leading to an increased pressure meaning the transverse velocity with which the system expands outwards should be slightly higher.

Lastly there is an increase of the coefficient for increasing transverse momenta up to 3-3.5 GeV/c after that the coefficient looks to be decreasing slowly. Furthermore there seems to be a mass dependence of the coefficient, because the protons have a higher maximum value than both pions and kaons which are much

lighter than the proton[12]. On the other hand there is no significant difference in the values of v_2 measured between kaons and pions for p_T >2.5 GeV/c. This is interesting since the mass of the kaon (approx. 494 Mev/c^2) is about 3.5 times larger than that of the pion (approx. 140 MeV/c^2). It could indicate that there is some sort of particle type grouping for values of p_T higher than 2.5 GeV/c, considering that kaons and pions are both mesons (consist of two quarks) and the protons are baryons (three quarks).

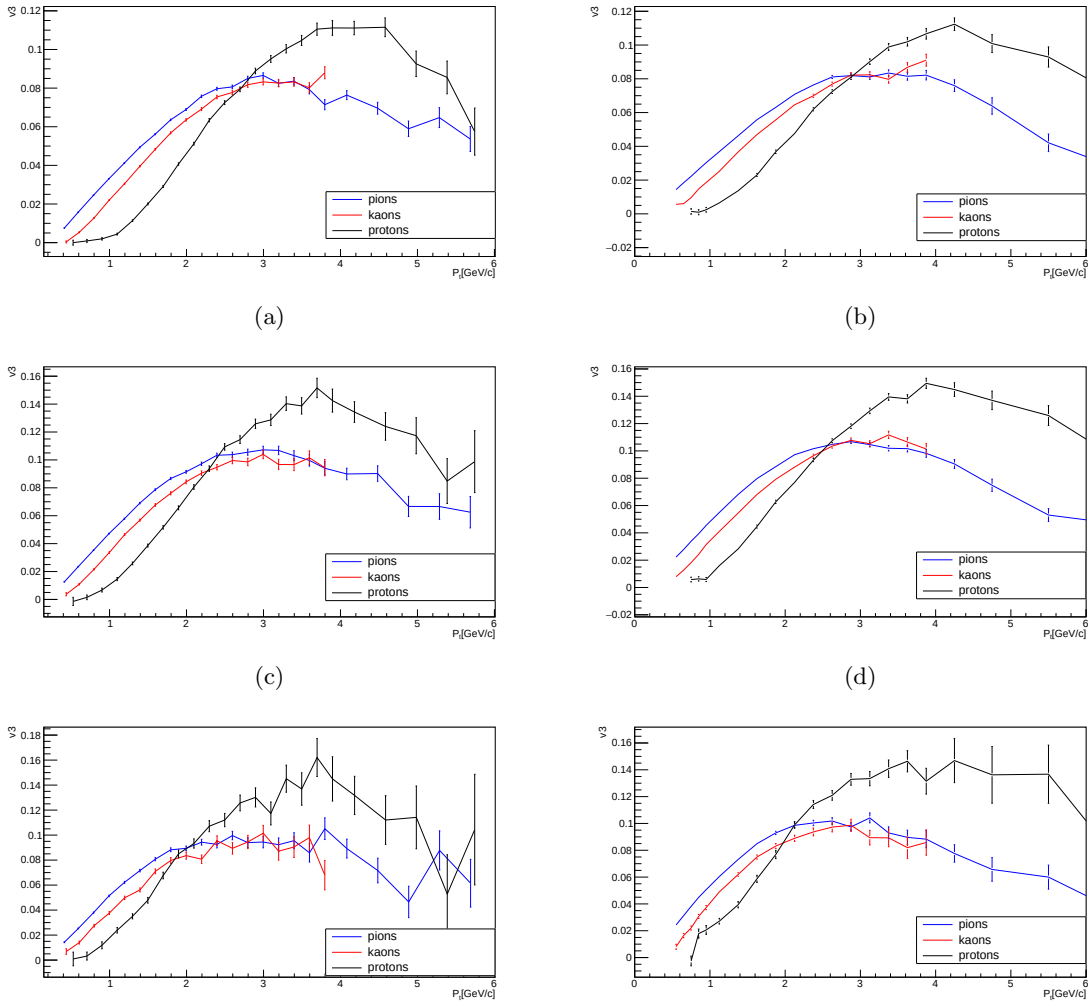

Figure 8: Triangular flow coefficients for various centralities: (a) and (b) at 0-5%; (c) and (d) at 20-30%; (e) and (f) at 40-50%

Figure 8 presents the triangular flow as a function of transverse momentum for all particle species. Similar to Figure 7 the left-hand side presents the plots for $\sqrt{s_{NN}} = 2.76$ TeV and the right-hand side presents the plots for $\sqrt{s_{NN}} = 5.02$ TeV. Analogous to v_2 there is a centrality dependence of the coefficient, although it is much less pronounced than with the v_2 coefficients. Therefore it seems that v_2 reflects the initial geometry of the system more than v_3 [12].

Based on Figures 6, 7 and 8 these results look in line with what would be expected. That is, the higher energy case results in a higher particle yield, but it doesn't affect so much the flow coefficients of the system. The flow is mostly affected by the initial geometry of the system (central or peripheral).

The plots from Figures 6, 7 and 8 have been used as an input for the blast-wave fit and the corresponding parameters (see Section 2.3) were extracted. In this thesis the average transverse velocity of the system $\langle\beta_T\rangle$,

the freeze-out temperature T_{fo} and the strength of the second-order oscillation of the transverse rapidity ρ_2 are discussed. Parameters T_{fo} and ρ_2 are directly extracted from the fit, but β_{T} is related to ρ_0 and is given by

$$\langle\beta_{\mathrm{T}}\rangle = \tanh(\frac{2}{3}\rho_0) \tag{3}$$

where ρ_0 is related to the boost strength.

5 Results

In Figure 9 the result of the blast-wave model fit for the spectra in centrality range 30-40% is presented, the fit results on the elliptic flow coefficient are presented in Figure 10 (also centrality range 30-40%). The other fit results can be found in Appendix A and B.

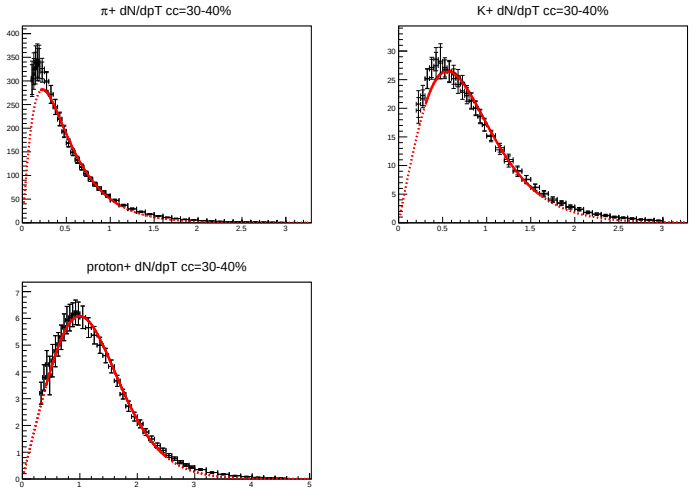

(a)

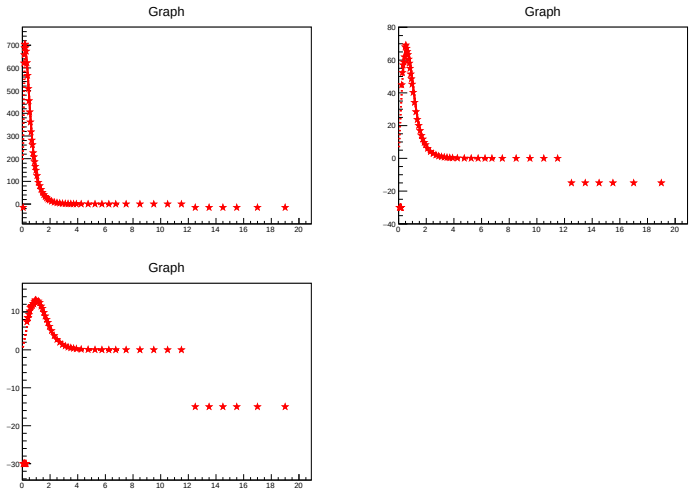

(b)

Figure 9: Fit results for 2.76 TeV and 5.02 TeV particle yield with centrality 30-40%

As mentioned the spectra for the $\sqrt{s_{NN}}$= 5.02 TeV data look a bit different this is due to the conversion of the data from histograms to graphs. As a result the fit is good for the first data points, but there is no fit done through the last points in the tail of the distribution. The fit for $\sqrt{s_{NN}}$ = 2.76 TeV is very good,

with a fit through all data points all the way through the tail too. Even though the fit for 5.02 TeV is not ideal with respect to the tail of the distribution, the parameters should be reliable and are therefore included in the results. The reason for this is that the parameter of the spectra depend on the shape of the spectra and the fits are good up to around 6 GeV/c (same as where the spectra for 2.76 TeV stop), after which the distribution is basically zero and the shape doesn't change.

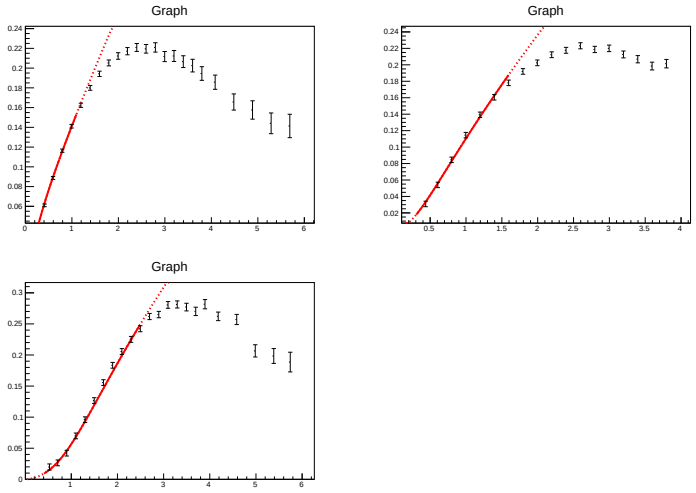

(a)

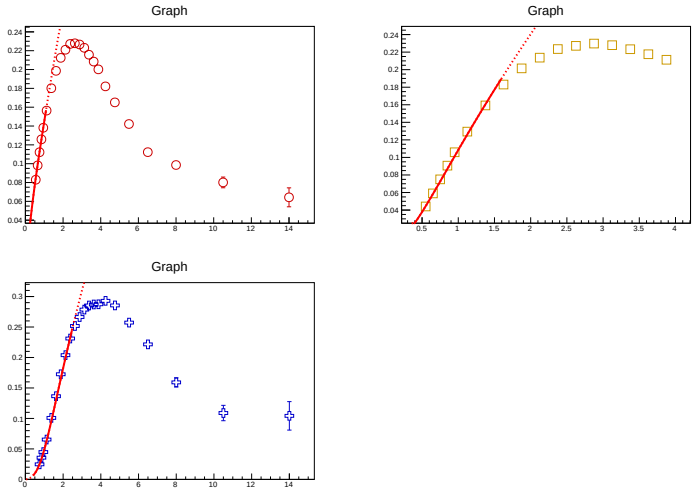

(b)

Figure 10: Fit results for v_2 at 2.76 TeV and 5.02 TeV with centrality 30-40%

From the parameter ρ_0 that was found through the fits the transverse velocity of the system for different centralities has been calculated (see Eq. 3). From Figure 11a there is not a significant difference in the determination of the transverse velocity through a singlefit or a doublefit.

In both Figures 11a and 11b there is a strong decline from 5-10% centrality and a little less strong in the interval 10-20% after which it again declines strongly with decreasing centrality. Figure 11c shows that there no change in the way the transverse velocity develops at different energies and that it is just the magnitude of the transverse velocity that slightly increases with increasing energy.

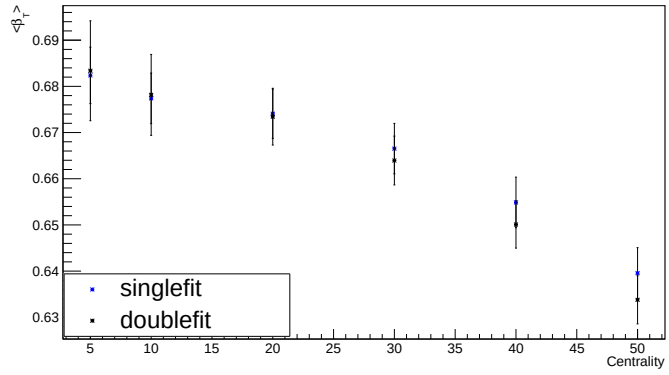

(a)

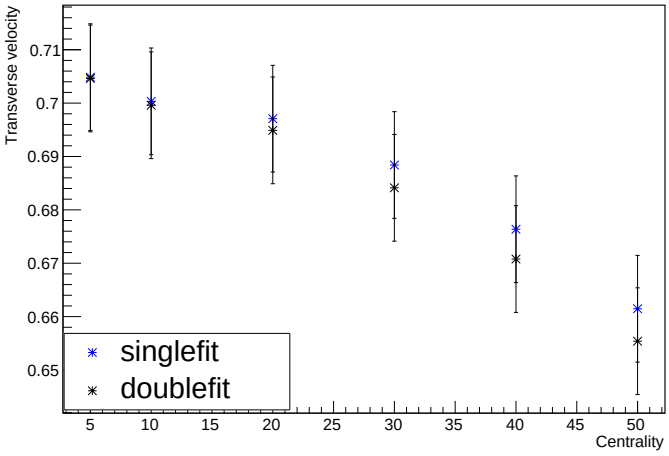

(b)

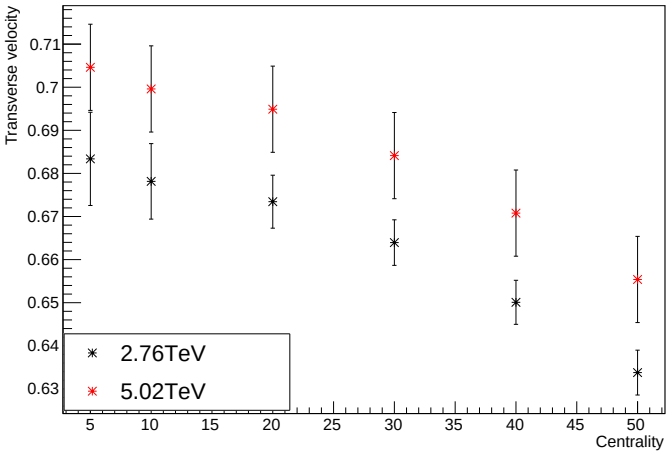

(c)

Figure 11: (a) Transverse velocity of the system at 2.76 TeV
(b) Transverse velocity of the system at 5.02 TeV
(c) Difference in transverse velocity at 2.76 TeV and 5.02 TeV as measured with a fit done on both spectra and v_2.

The parameter T_{fo} that was found with the blast-wave model is plotted in Figure 12 as a function of the transverse velocity.

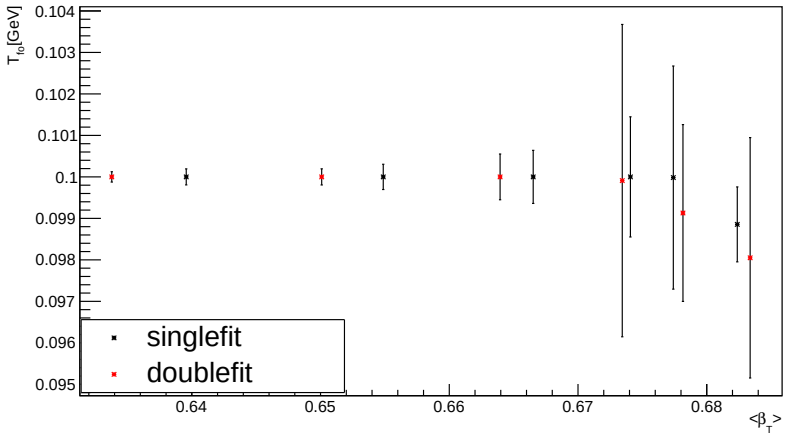

(a)

(b)

Figure 12: T_{fo} as a function of transverse velocity at (a) 2.76 TeV and (b) 5.02 TeV

From Figure 12 it does seem to be the case that the freeze-out temperature is neither dependent on the energy of the collision or the transverse velocity of the system.

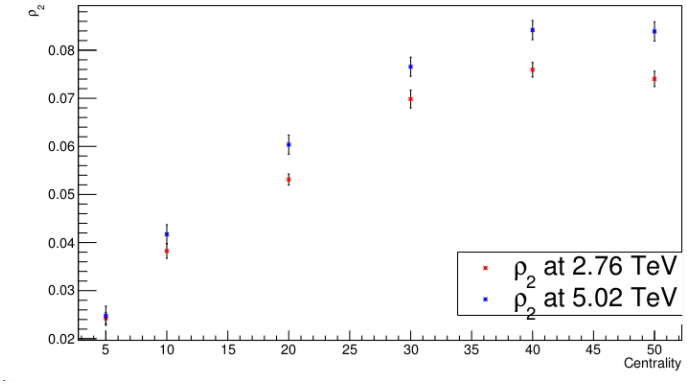

Figure 13: Parameter ρ_2 as a function of centrality

Parameter ρ_2, plotted in Figure 13 displays the same behaviour as the elliptic coefficient v_2; it increases with decreasing centrality until a certain point (30-40%) then it starts to decrease/flat out. This is what was expected because ρ_2 is related to the elliptic flow.

5.1 Triplefit

With the blast-wave model a fit on the spectra, v_2 and v_3 (triplefit) was also done, however these fits are not good enough to give reliable results. The fits miss the data points for low p_T values. For centrality 30-40% the fits are shown in Figure 14, the other fit results can be found in Appendix C. Especially the fits for kaons and protons are not through the data points at all. It does indicate that the blast-wave fit does not seem to work for the spectra, v_2 and v_3 simultaneously.

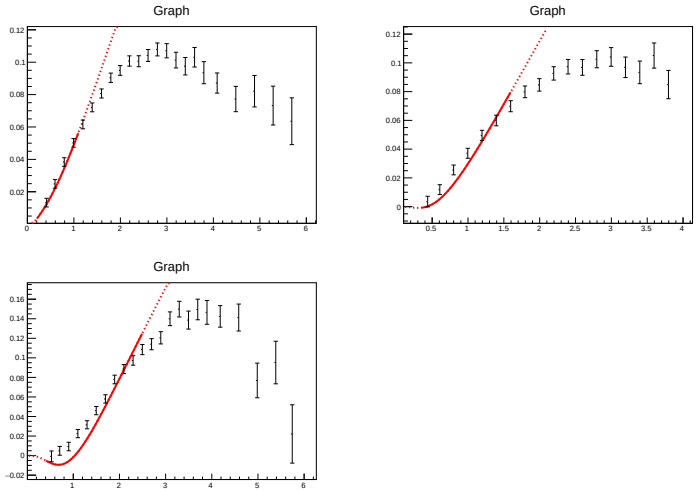

(a)

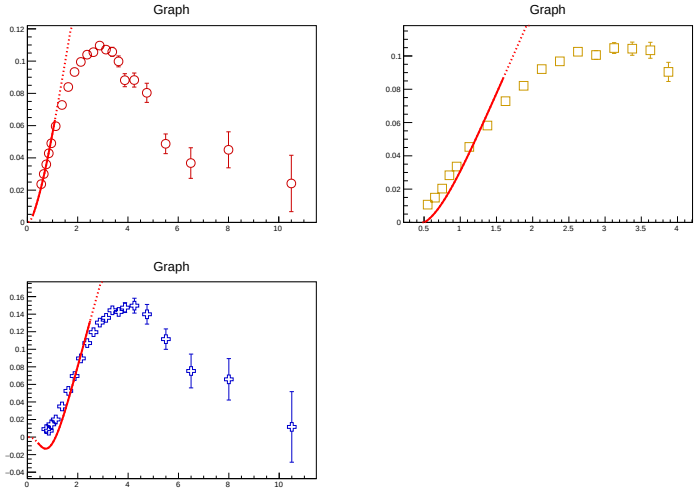

(b)

Figure 14: Fit results for v_3 with centrality 30-40%

6 Discussion and Conclusion

Especially for $\sqrt{s_{NN}}$= 2.76 TeV the blast-wave model works rather accurately on both the single- and doublefit. This seems to be the case for $\sqrt{s_{NN}}$= 5.02 TeV too; the fits are good on the spectra and v_2. However, the error propagation from the uncertainties given by the fit are too insignificant when compared to the results and uncertainties for $\sqrt{s_{NN}}$= 2.76 TeV. Thus instead the uncertainties from figures 11b, 12b and 13 are the same order of magnitude as the uncertainties determined for $\sqrt{s_{NN}}$= 2.76 TeV. It might be necessary to review the input from 5.02 TeV, as the spectra had to be converted from histograms to graphs this might have been the reason for the insignificance of the uncertainties. In addition to the conversion that had to be done the p_T range is different for both energies. In the case of 2.76 TeV the spectra and v_2 had a p_T range up to 6 GeV/c whereas the spectra and v_2 for 5.02 TeV had a p_T up to 14 GeV/c. For the v_2 this doesn't seem to have a great impact on the fit, because the model fits up to 1-2 GeV/c. However it might have a greater influence on the fit of the spectra, for the reason that the spectra of 5.02 TeV show discontinuity after 6 GeV/c. So when the tail of this distribution is left out the fit on the spectra could maybe be improved.

Besides, this discussion on the fit on the spectra the results for the single- and doublefit are in line with expectations. The transverse velocity shows a slight increase with increasing energy, so does parameter ρ_2 and a value of T_{fo} independent of centrality consistent with similar studies.

Remarkable is the fact that the blast-wave model is incapable of fitting the spectra, elliptic flow and the triangular flow simultaneously (see Figure 14a). So it is of interest to take a closer look at the model; are the assumptions from the RL model not justified any longer? Or perhaps it needs some modifications in the description of the parameters. For now the higher order flow coefficients can not be parameterized with the blast-wave model and it is relevant to investigate whether it is a defect in the model or whether it is physical aspect of the heavy-ion collision.

A Fit Results for the Spectra

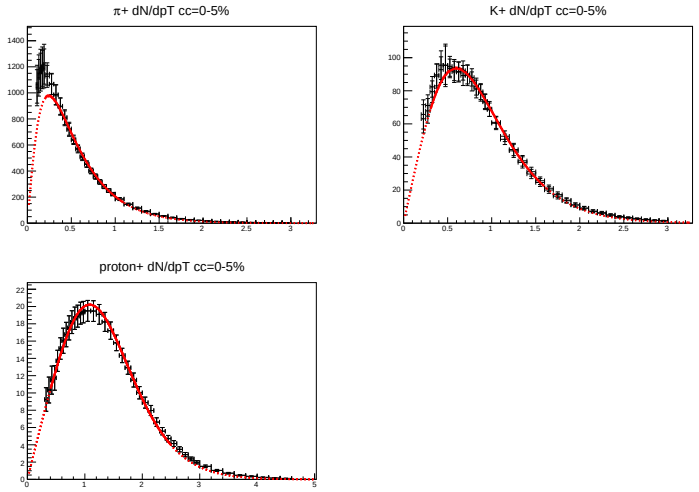

(a)

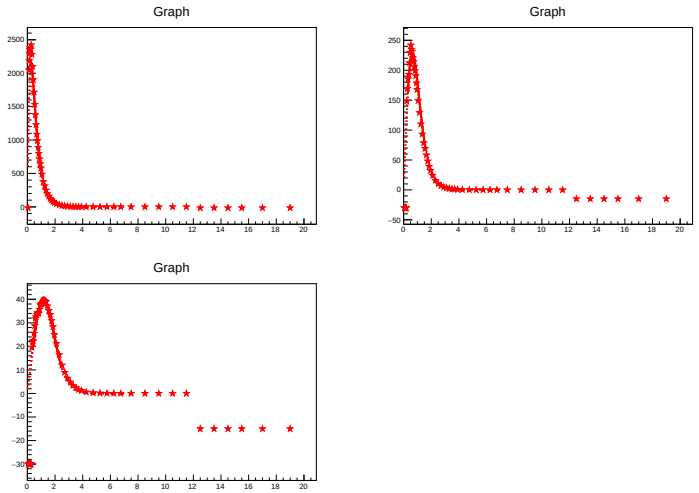

(b)

Figure 15: Fit results for centrality range 0-5%

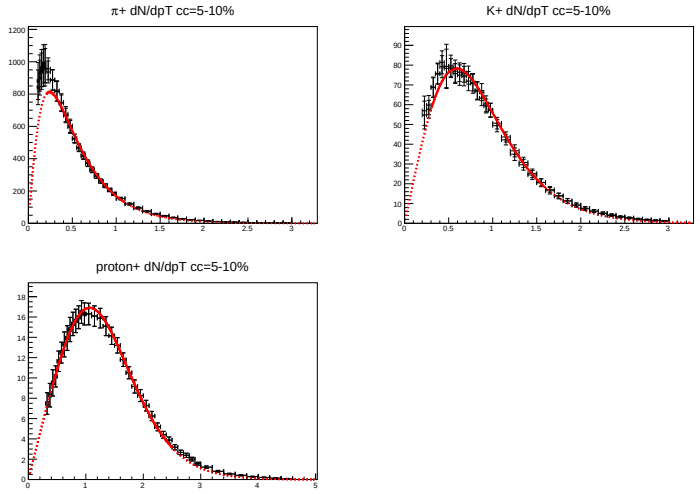

(a)

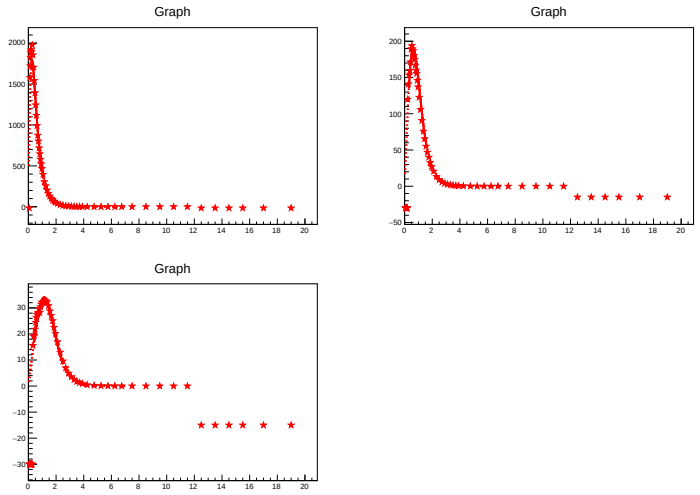

(b)

Figure 16: Fit results for centrality range 5-10%

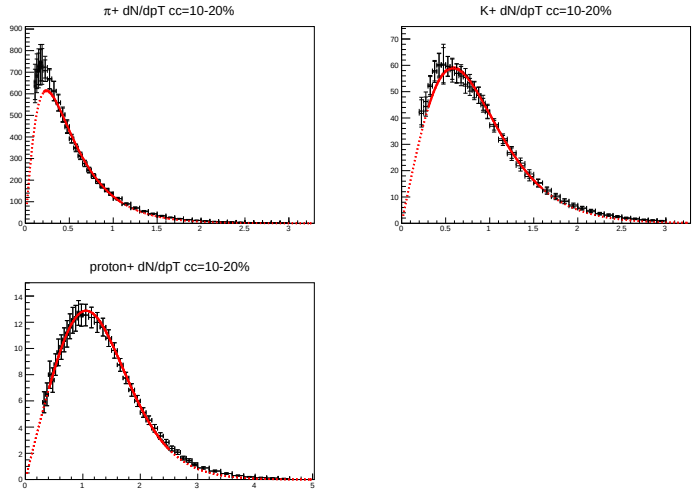

(a)

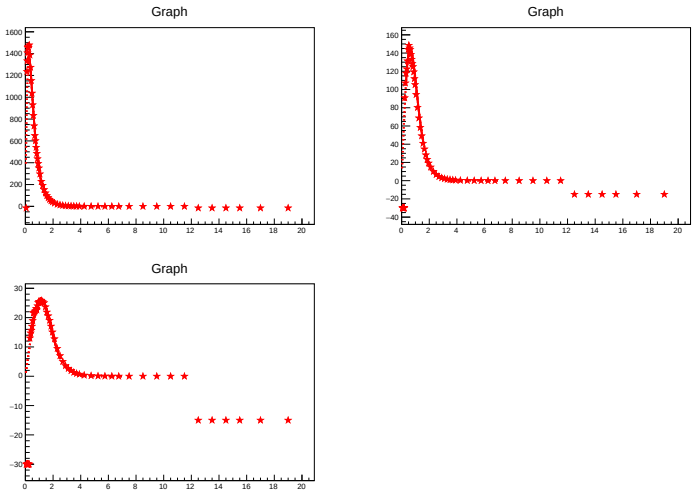

(b)

Figure 17: Fit results for centrality range 10-20%

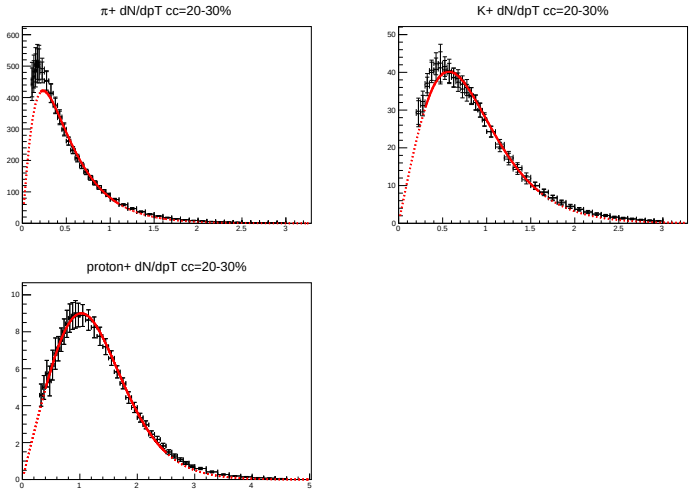

(a)

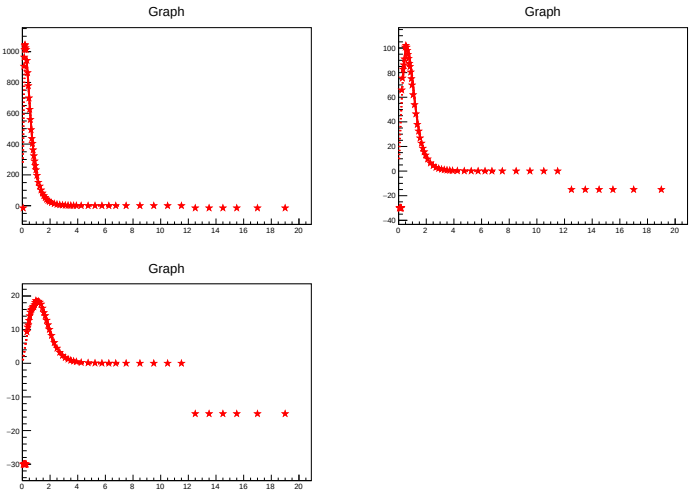

(b)

Figure 18: Fit results for in centrality range 20-30%

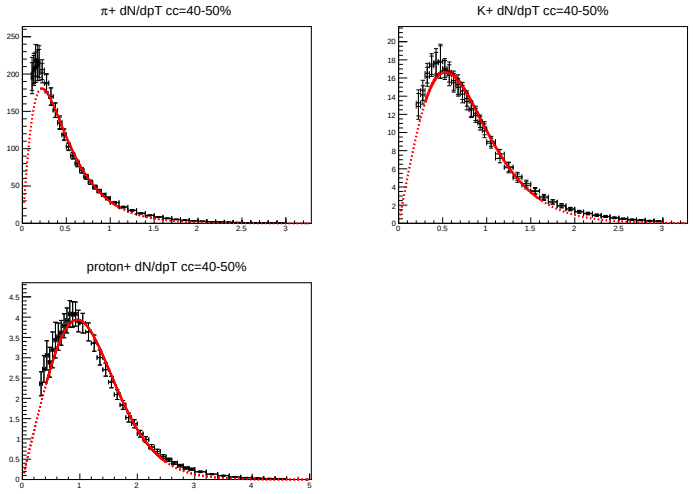

(a)

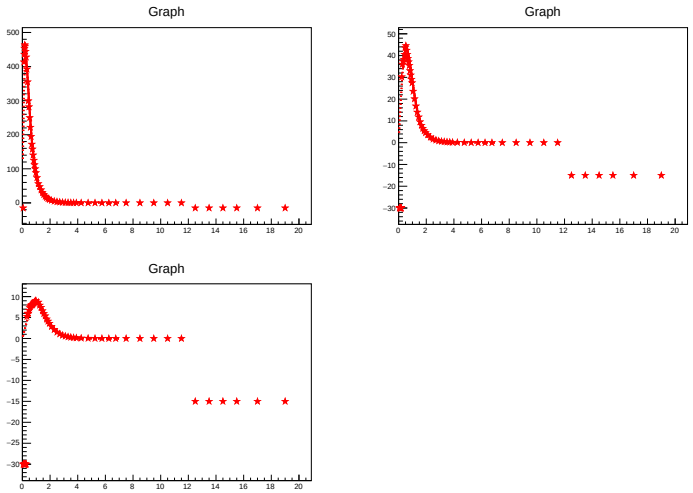

(b)

Figure 19: Fit results for centrality range 40-50%

B Fit Results for Elliptic Flow

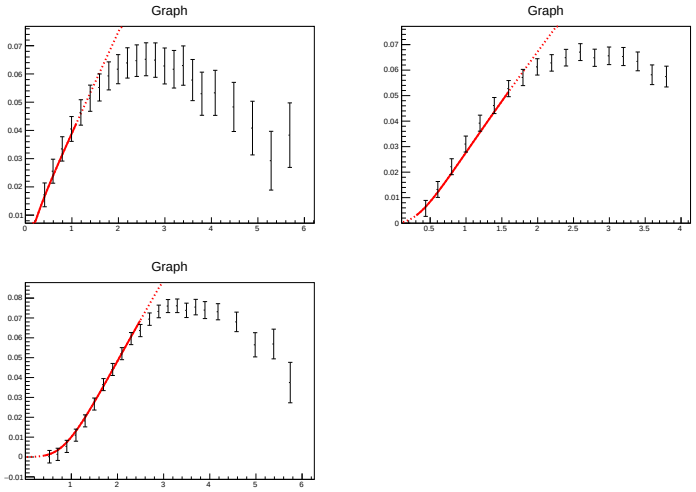

(a)

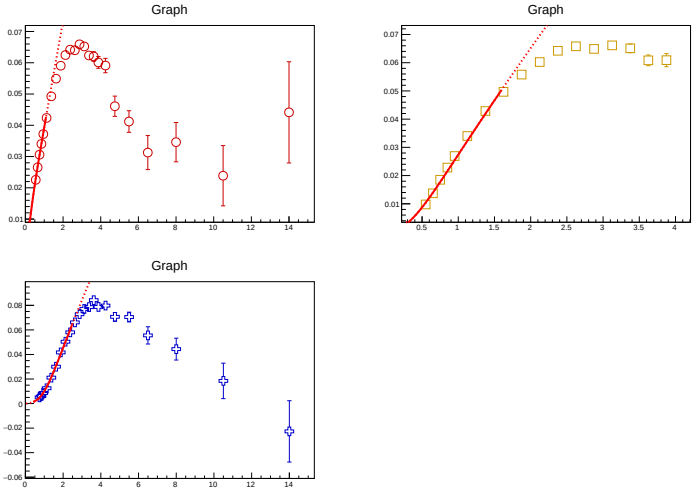

(b)

Figure 20: Fit results for centrality range 0-5%

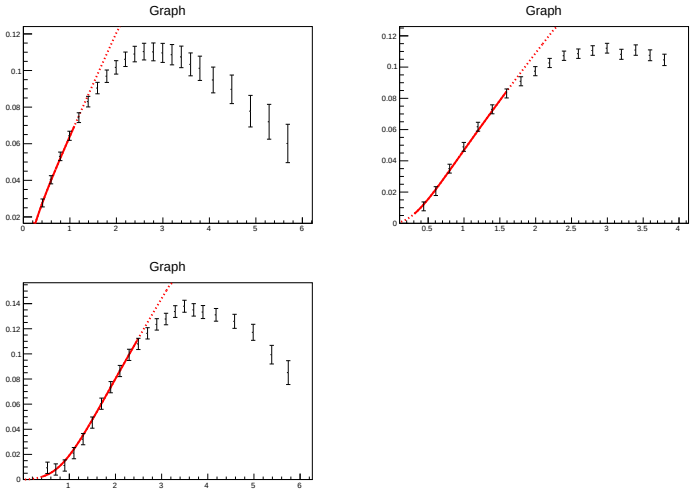

(a)

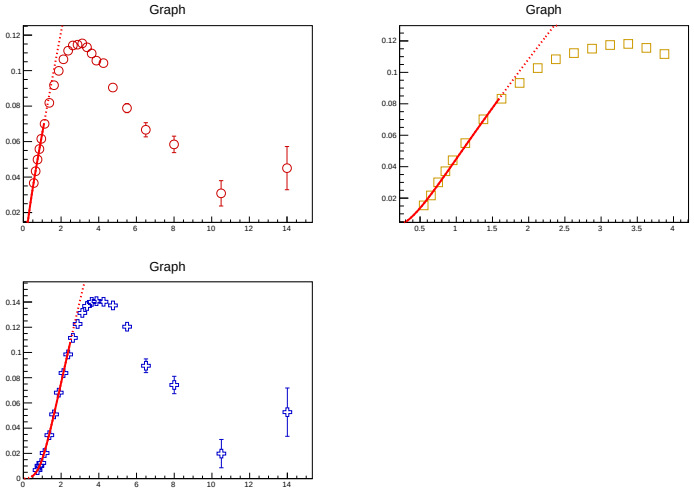

(b)

Figure 21: Fit results for centrality range 5-10%

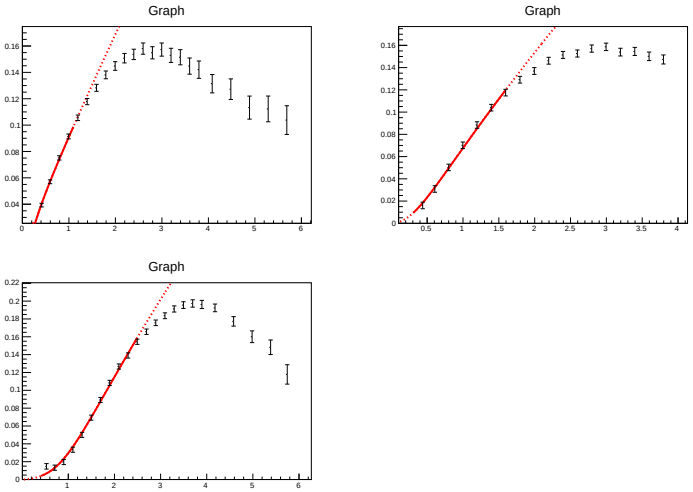

(a)

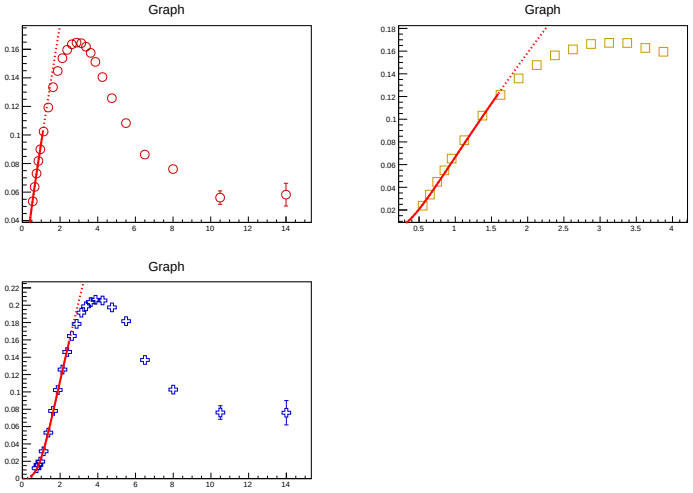

(b)

Figure 22: Fit results for centrality range 10-20%

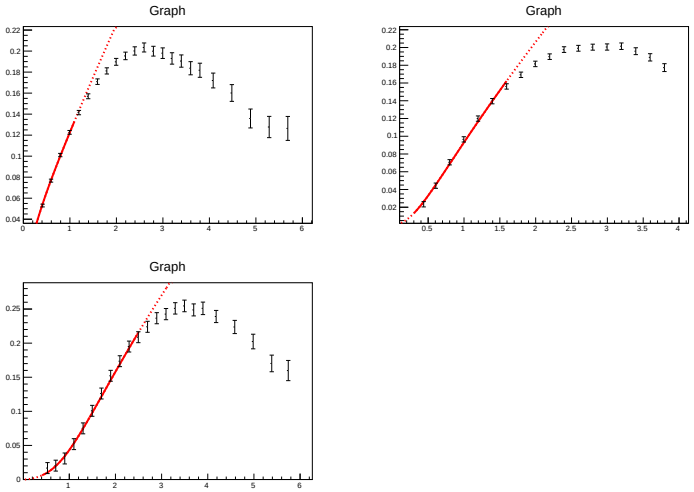

(a)

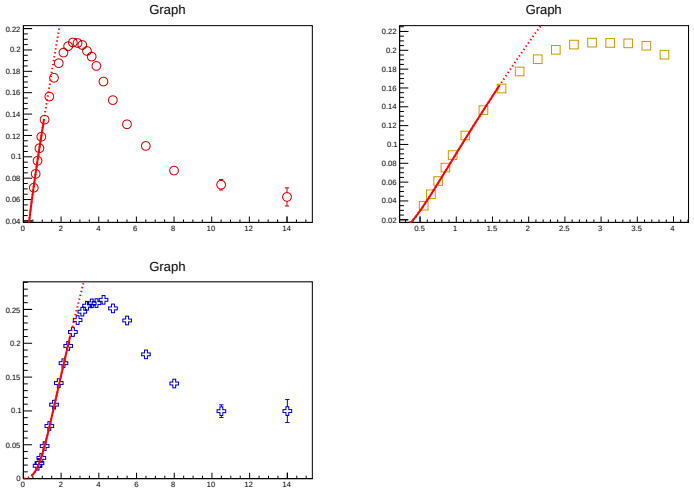

(b)

Figure 23: Fit results for centrality range 20-30%

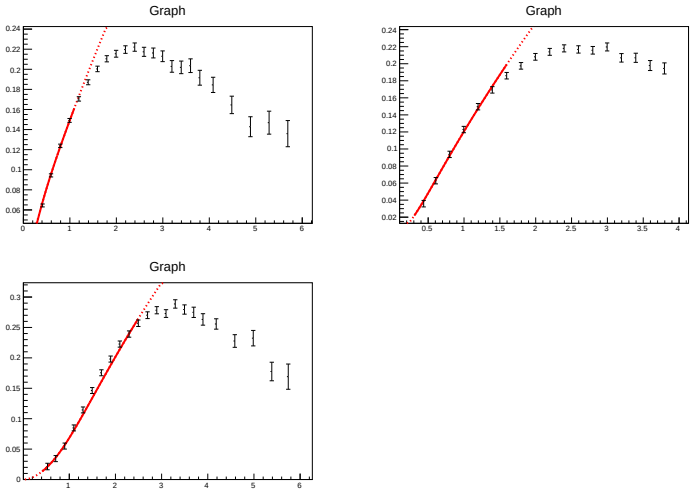

(a)

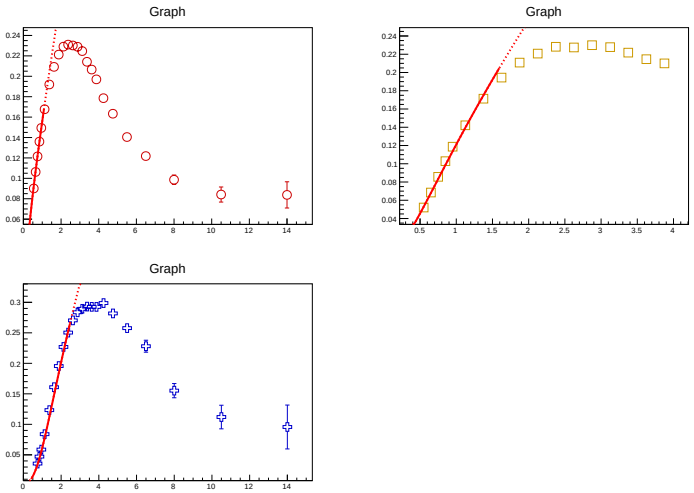

(b)

Figure 24: Fit results for centrality range 40-50%

C Fit Results for Triangular Flow

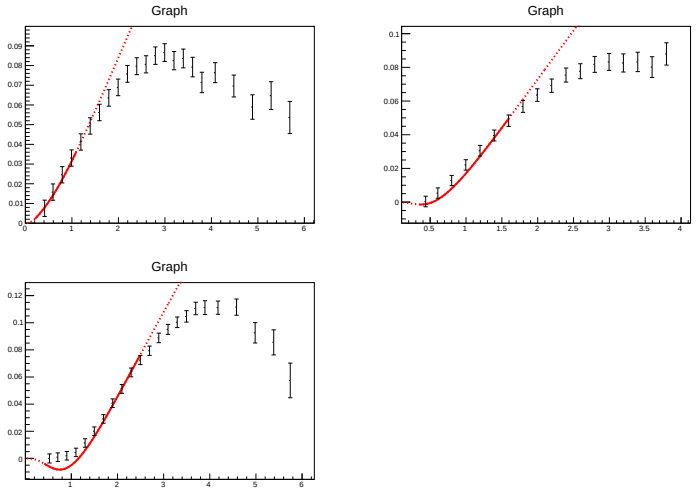

(a)

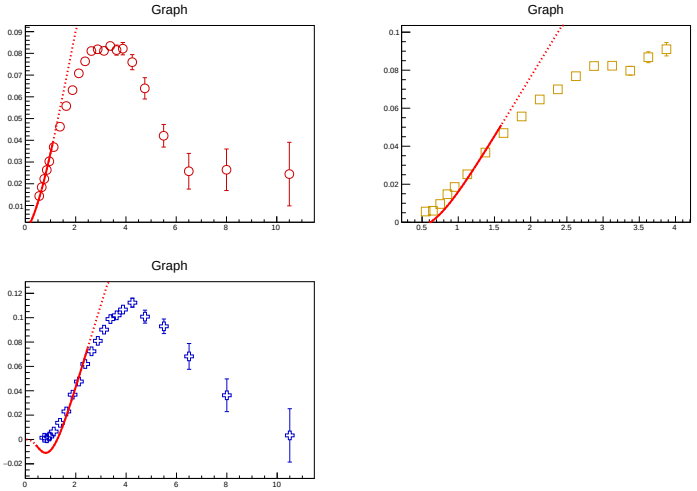

(b)

Figure 25: Fit results for centrality range 0-5%

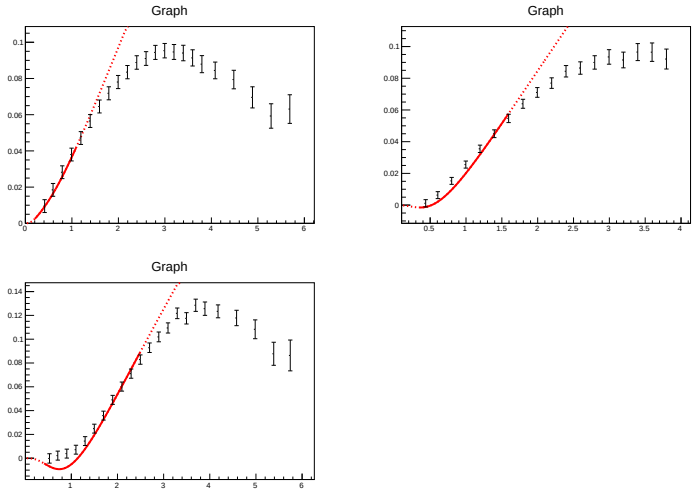

(a)

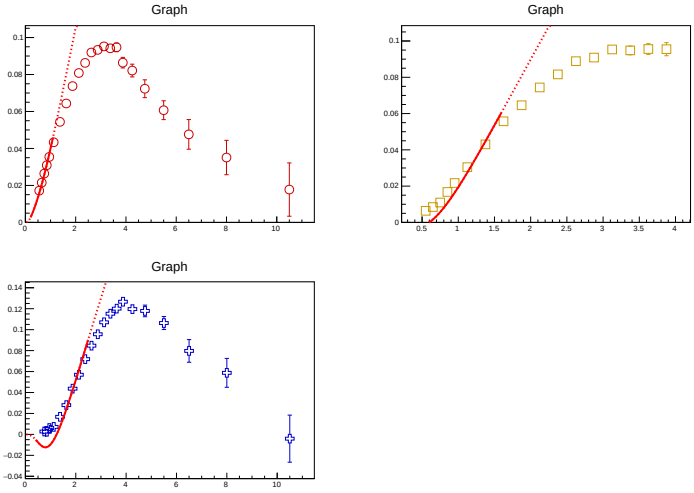

(b)

Figure 26: Fit results for centrality range 5-10%

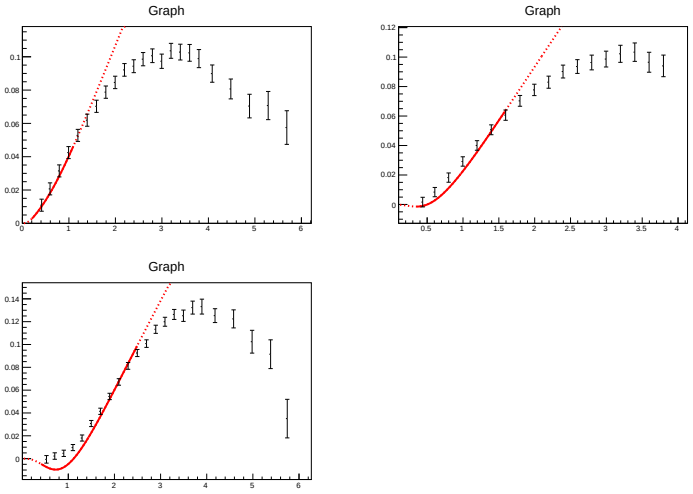

(a)

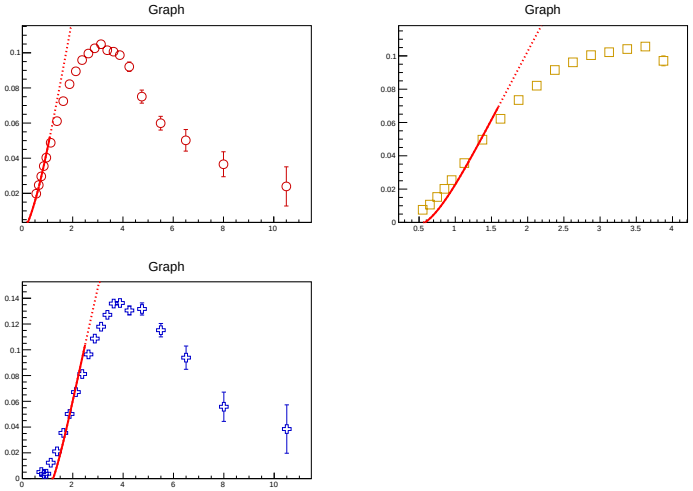

(b)

Figure 27: Fit results for centrality range 10-20%

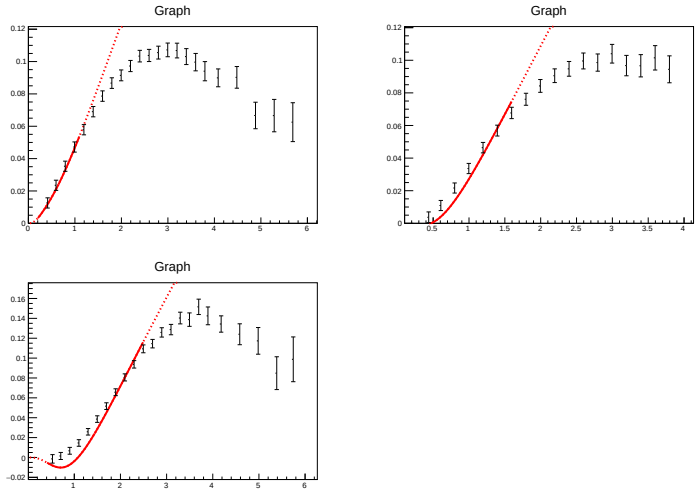

(a)

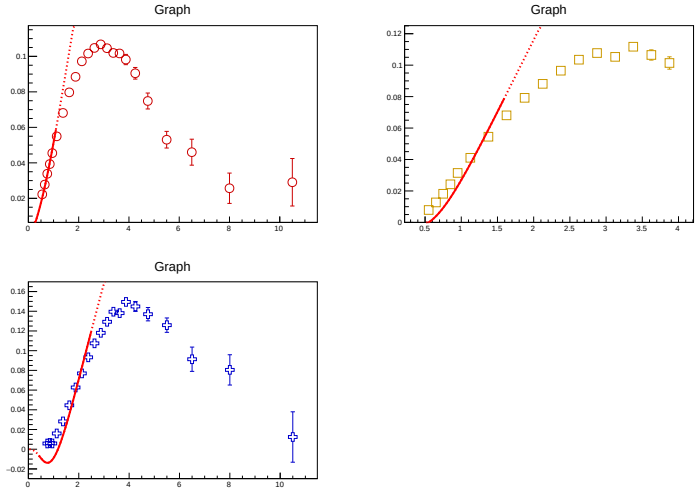

(b)

Figure 28: Fit results for centrality range 20-30%

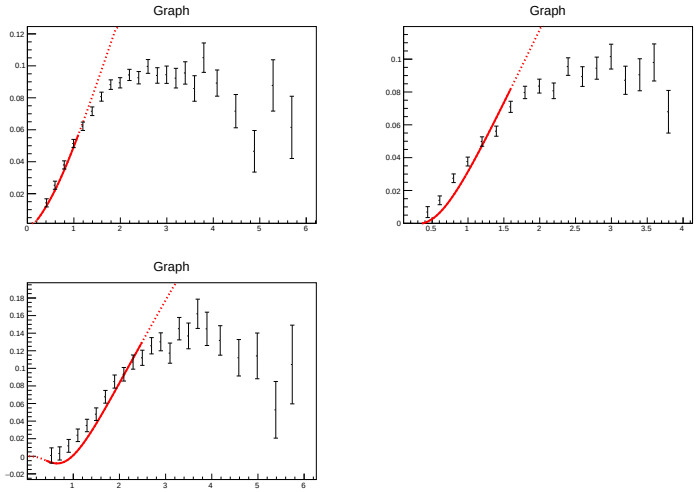

(a)

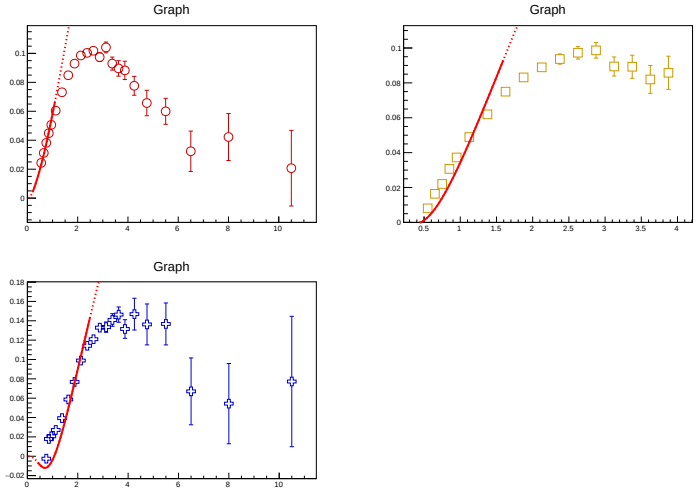

(b)

Figure 29: Fit results for centrality range 40-50%

References

[1] Last visited January 6, 2018, URL https://en.wikipedia.org/wiki/Standard_Model#/media/File:Standard_Model_of_Elementary_Particles.svg.

[2] *The Standard Model* (2012), URL http://cds.cern.ch/record/1997201.

[3] R. S. Bhalerao, pp. 219–239. 21 p (2014), comments: Updated version of the lectures given at the First Asia-Europe-Pacific School of High-Energy Physics, Fukuoka, Japan, 14-27 October 2012. Published as a CERN Yellow Report (CERN-2014-001) and KEK report (KEK-Proceedings-2013-8), K. Kawagoe and M. Mulders (eds.), 2014, p. 219. Total 21 pages, URL https://cds.cern.ch/record/1695331.

[4] *Heavy ions and quark-gluon plasma* (2012), URL http://cds.cern.ch/record/1997370.

[5] J. Adam et al. (ALICE), Phys. Rev. **C93**, 034913 (2016), 1506.07287.

[6] A. Toia, CERN Courier (2013), URL http://cerncourier.com/cws/article/cern/53089.

[7] F. Retiere and M. A. Lisa, Phys. Rev. **C70**, 044907 (2004), nucl-th/0312024.

[8] *The Large Hadron Collider* (2014), URL http://cds.cern.ch/record/1998498.

[9] F. Carminati, P. Foka, P. Giubellino, A. Morsch, G. Paic, J.-P. Revol, K. Safark, Y. Schutz, and U. A. Wiedemann (ALICE Collaboration), Journal of Physics G: Nuclear and Particle Physics **30**, 1517 (2004), URL http://stacks.iop.org/0954-3899/30/i=11/a=001.

[10] Last visited on January 6, 2018, URL http://aliceinfo.cern.ch/Public/en/Chapter2/Chap2InsideAlice-en.html.

[11] B. Abelev et al. (ALICE), Phys. Rev. **C88**, 044910 (2013), 1303.0737.

[12] J. Adam et al. (ALICE), JHEP **09**, 164 (2016), 1606.06057.

[13] ALICE, *Preliminary results for particle production and flow coefficients from Pb-Pb collisions at 5.02 TeV*, yet to be published.